

# SnapGen-V: Generating a Five-Second Video within Five Seconds on a Mobile Device

Yushu Wu<sup>1,2†</sup> Zhixing Zhang<sup>1,3†</sup> Yanyu Li<sup>1†‡</sup> Yanwu Xu<sup>1</sup> Anil Kag<sup>1</sup> Yang Sui<sup>1</sup>  
 Huseyin Coskun<sup>1</sup> Ke Ma<sup>1</sup> Aleksei Lebedev<sup>1</sup> Ju Hu<sup>1</sup> Dimitris N. Metaxas<sup>3</sup>  
 Yanzhi Wang<sup>2</sup> Sergey Tulyakov<sup>1</sup> Jian Ren<sup>1‡</sup>

<sup>1</sup>Snap Inc.

<sup>2</sup>Northeastern University

<sup>3</sup>Rutgers University



Figure 1. **Example generation results from our mobile text-to-video model.** Our model can generate high-quality and motion consistent 5-second videos on a *mobile* device (e.g., iPhone 16 Pro Max) within 5 seconds.

## Abstract

We have witnessed the unprecedented success of diffusion-based video generation over the past year. Recently proposed models from the community have wielded the power to generate cinematic and high-resolution videos with smooth motions from arbitrary input prompts. However, as a supertask of image generation, video generation models require more computation and are thus hosted mostly on cloud servers, limiting broader adoption among content creators. In this work, we propose a comprehensive acceleration framework to bring the power of the large-scale video diffusion model to the hands of edge users. From the network architecture scope, we initialize from a compact image backbone and search out the design and arrangement of temporal layers to maximize hardware efficiency. In addition, we propose a dedicated adversarial fine-tuning algorithm for our efficient model and reduce the denoising steps to 4. Our model, with only 0.6B parameters, can generate a 5-second video on an iPhone 16 PM within 5 seconds. Compared to server-side models that take minutes on powerful GPUs to generate a single video, we accelerate the generation by magnitudes while delivering on-par quality. Project page at <https://snap-research.github.io/snapgen-v/>.

## 1. Introduction

Recently, the rapid advancement of video diffusion models [4] inspires revolutions in content creation. With the emergence of video models from industry [41] and research community [67], content creators can animate a static image [3] or generate cinematic videos from arbitrary prompts [55, 67, 78]. Video diffusion models also enable downstream applications like video editing [12, 20, 30], novel view synthesis [25, 57], and multi-modal generation [56].

Despite the success in generation quality, the huge number of parameters and slow generation speed prohibit the wide deployment of video diffusion models. For instance, CogVideoX-5B [67] generates a video (49 frames at 8 fps,  $720 \times 480$  resolution) in 5 minutes with 50 inference steps on an NVIDIA A100 GPU. Compared to text-to-image diffusion models [45], video diffusion models require extra parameters to model sophisticated motions [3, 13, 62]. In addition, video data usually incurs higher spatial-temporal resolution for UNet denoisers [3, 13], or equivalently more tokens for DiT models [40], which adds up to the computation complexity. Recent works explore efficient model architectures and attention mechanisms for image diffusion models [8, 64, 70]. However, there is little effort in the literature dedicated to accelerating and deploying video models at scale, especially for mobile devices.

In this work, we systematically investigate the redundancies in video diffusion models and propose a mobile

<sup>†</sup>Equal contribution

<sup>‡</sup>Corresponding authors

acceleration framework. First, we obtain an efficient spatial backbone by following prior works [11, 29] to prune a pre-trained text-to-image diffusion model [45]. The pruned model achieves  $2.5\times$  size compression and more than  $10\times$  speedup compared to Stable Diffusion v1.5 [45], while maintaining comparable generative quality. Starting from a pre-trained image model offers two key benefits: (i) it eliminates the need for costly large-scale pre-training, and (ii) with a compact image model, we can significantly narrow the search space in subsequent stages, focusing only on optimizing temporal layers, and thereby accelerating the discovery of the final model architecture.

Even with the efficient image backbone, applying previous temporal inflation methods [3, 4, 13] still results in tremendous computation cost and encounters out-of-memory issues on mobile. Thus, our second stage is to systematically investigate different types of temporal layers and perform a latency-memory joint search to determine the spatial-temporal architecture for efficient mobile deployment. Unlike previous methods [3, 4, 13] that typically rely on a specific type of temporal modeling layer, we investigate all possible designs, including temporal attention, spatial-temporal full attention (3D attention), temporal cross attention, and temporal convolutions (Conv3D). Besides, our search space includes the position (resolution) to apply these temporal layers, and number of layers to use (in Sec. 3.2). We profile the computation, memory footprint, and on-device latency of architecture candidates, and perform evolutionary search to discover the architecture with Pareto optimality of speed and quality. The searched network is only 0.6B in size, and can generate a 5-second video clip on iPhone 16 PM without hitting memory bound. In contrast, all prior video diffusion models fail to run on mobile, even for the smallest open-sourced ones like the 16-frame AnimateDiff [13] and 14-frame SVD [3] (Tab. 1).

Finally, to further speed up generation on mobile, we distill our efficient video diffusion model with a tailored adversarial fine-tuning method capable of image-video mixed training. We reduce the number of denoising steps from 25 to 4, and eliminate classifier-free guidance [16], leading to more than  $12\times$  speedup without performance degradation. As in Tab. 1, our *mobile* speed is faster than most GPU-deployed (e.g., on A100) counterparts.

Model	Type	Steps	Params (B)	A100 (s)	iPhone (s)	Vbench ( $\uparrow$ )
OpenSora-v1.2	DiT	30	1.2	31.00	$\times$	79.76
CogVideoX-2B	DiT	50	1.6	54.09	$\times$	80.91
AnimateDiff-V2	UNet	25	1.2	9.04	$\times$	80.27
AnimateDiffLCM	UNet	4	1.2	1.77	$\times$	79.42
Ours	UNet	4	0.6	0.47	4.12	81.14

Table 1. Comparison of size (number of parameters), speed (tested on NVIDIA A100 and iPhone 16 Pro Max), and performance (on VBench [19]) for various models.

With the proposed framework, we successfully deploy our 0.6B text-to-video model on an iPhone 16 Pro Max, achieving the generation of a 5-second video clip within 5 seconds. This work represents not only the very *first* mobile deployment attempt of the video diffusion model, but also demonstrates its real-time potential<sup>1</sup>. Our contributions are summarized as follows:

- Through image-video joint training, spatial and temporal architecture design, and mobile-driven latency-memory joint architecture search, we develop a comprehensive mobile acceleration framework for the text-to-video diffusion model.
- We propose an adversarial fine-tuning technique tailored for video diffusion models. Despite the already compact nature of our mobile denoiser, we further distill it to 4 denoising steps with superior quality.
- Our work is the very first one to show the possibility of real-time text-to-video generation on mobile devices, unlocking the possibility of deploying applications of video diffusion models at scale.

## 2. Related Work

**Video Diffusion Models.** Denoising Diffusion Probabilistic Models [17] is the trending paradigm for building video diffusion models, demonstrating photorealistic quality and generic generation capabilities. Pioneer works often start from a pre-trained text-to-image diffusion model [45] and insert temporal layers to model motions along frame sequence [3, 4, 13, 62, 75]. In addition, training-free noise tuning techniques are proposed to ease the alignment between frames [23, 34, 43, 63, 73]. Later, with the emergence of large-scale, high-quality video datasets [7, 38] and Transformer backbones [40], subsequent works curate their own dataset and build large video diffusion models with exceptional quality, such as the open-sourced CogVideoX [67], Mochi 1 [55], PyramidalFlow [21], Allegro [78], and close-sourced ones including Hailuo [37], Runway Gen 3 Alpha [46], Kling [24], Luma Dream Machine [1], Pika 1.5 [2], Sora [39], and MovieGen [41]. Remarkably, the open-sourced projects Open-Sora [77] and Open-Sora-Plan [26] provide the community with reliable implementations to replicate large-scale video diffusion models.

Dividing by task type, video diffusion models can be categorized into text-to-video generation [5, 6, 13, 15, 18, 21, 27, 28, 42, 55, 56, 67, 78], image-to-video generation [3, 79], or specific motion controls [14, 44, 61, 71, 76]. Though some work [8, 29, 70, 73] aim to improve the efficiency of diffusion models, the acceleration for mobile deployment of video diffusion models is still in absent. Popular video models [21, 55, 67] can only run on server-level

<sup>1</sup>This work performs conventional T2V generation, generating an entire video at once. However, a more suitable real-time capability would involve streamlined, continuous video generation, which we leave for future work.

GPUs to generate videos in tens of seconds or even minutes. **Step Distillation** brings almost linear generation speedup for diffusion models. Early work [29, 47] progressively distill a student network to predict a further ODE location with teacher guidance, resulting in fewer inference steps, while Consistency Models [52, 53] and Rectified Flow [33] refine the prediction objective to clean data or global velocity to achieve fewer-step inference. Later works [50, 51, 65] further incorporate adversarial loss to distill a single-step student, and enhance multi-step results as well.

Despite extensive research in image diffusion models [9, 22, 36, 59, 66, 68, 69], step distillation for video diffusion model is under-explored. One type of work applies consistency distillation to generate videos in 4 steps [58, 60, 72]. Another trend adopts adversarial distillation to achieve few-step (1-2) generation [32, 35, 74]. However, these methods distill pre-trained large models with enough redundancy along the trajectory, while we find them not applicable to our efficient model and yield inferior performance.

### 3. Method

Our objective is to achieve high-fidelity and temporally consistent video generation on mobile devices. However, current text-to-video diffusion models face two key challenges in reaching this goal: (a) the memory and computation requirement is beyond the capability of even the most powerful mobile chips, *i.e.* iPhone A18 Pro, and (b) denoising with dozens of steps to generate a single output further slows down the process. To address these challenges, we propose a three-stage framework to accelerate video diffusion models on the mobile platform. First, we prune from a pre-trained text-to-image diffusion model to obtain an efficient spatial backbone. Second, we inflate the spatial backbone with a novel combination of temporal modules which are searched out with our mobile-oriented metrics. Finally, through adversarial training, our efficient model attains the capability to generate high-quality videos in only 4 steps.

#### 3.1. Preliminaries

Following [77], we employ a spatial-temporal VAE to compress image and video data into the latent space. Given video or image data  $\mathbf{v} \in \mathbb{R}^{n \times 3 \times H \times W}$ , where  $n$  is the number of frames with height  $H$  and width  $W$ , the spatial-temporal encoder,  $\mathbf{E}$ , maps the data to a latent space. The encoded frames are represented as  $\mathbf{x}_0 = \mathbf{E}(\mathbf{v})$ , resulting in  $\mathbf{x}_0 \in \mathbb{R}^{\tilde{n} \times 4 \times \tilde{H} \times \tilde{W}}$ . Here,  $\mathbf{x}_0 \sim p_{data}(\mathbf{x}_0)$  is a 4-channel latent, with a temporal compression of  $\tilde{n} = n/4$ , and spatial compression as  $\tilde{H} = H/8$ ,  $\tilde{W} = W/8$ .

We follow Rectified Flow [59] to train our latent diffusion model. According to the flow-matching-based diffusion form, the intermediate noisy state  $\mathbf{x}_t$  is defined as:

$$\mathbf{x}_t = (1 - t) \mathbf{x}_0 + t \epsilon, \text{ where } \epsilon \sim \mathcal{N}(0, I), \quad (1)$$

which is a linear interpolation between the data distribution and a standard normal distribution. The model aims to learn a vector field  $v_\theta(t, \mathbf{x}_t)$  using the Conditional Flow Matching objective, *i.e.*,

$$\mathcal{L} = \mathbb{E}_{t, \epsilon, \mathbf{x}_0} \|v_\theta(t, \mathbf{x}_t) - u_t(\mathbf{x}_t | \mathbf{x}_0)\|_2^2, \quad (2)$$

where  $u_t(\mathbf{x}_t | \mathbf{x}_0) = \epsilon - \mathbf{x}_0$ . Following [10], during training, we sample  $t$  from a logit-normal distribution, *i.e.*,

$$\pi(t; m, s) = \frac{1}{s\sqrt{2\pi}} \frac{1}{t(1-t)} \exp\left(-\frac{(\text{logit}(t) - m)^2}{2s^2}\right), \quad (3)$$

where  $\text{logit}(t) = \log \frac{t}{1-t}$ ,  $m$  and  $s$  are the location parameter and scale parameter, respectively.

#### 3.2. Hardware Efficient Model Design

**Spatial Backbone.** We follow [11, 29] to first prune an efficient text-to-image model as the spatial backbone. Specifically, we start from Stable Diffusion v1.5 [45], and borrow the knowledge from prior arts [29] to remove the most mobile-unfriendly attentions. We then prune the network depth and width following [11] and achieve  $\times 2.5$  size reduction and more than  $10\times$  speedup on mobile devices. We include qualitative visualizations of our image model in the *supplementary material*. Note that we use a UNet denoiser [17], leaving the exploration of DiT [40] to future work. The hierarchical structure of the UNet denoiser forms a good search space to achieve mobile efficiency, while the computation complexity of DiT grows quadratically with the number of tokens (generation resolution), making it challenging for mobile deployment.

**Temporal Layer Design.** Current latent video diffusion models typically adopt temporal self-attentions [13], cross-attentions [77], and convolutions [3] to model temporal dependencies. CogVideoX [67] demonstrates significant performance gain by using full 3D-Attention, at the cost of more computations and memory consumption. In this work, we enumerate and investigate all types of temporal modeling methods, including *Conv1D*, *Conv3D*, *SelfAttention1D*, *SelfAttention3D*, *CrossAttention1D*, and *CrossAttention3D*, and profile their complexity in Fig. 3. For instance, *SelfAttention1D* only models temporal dependency on a single coordinate, while *SelfAttention3D* models global dependencies and has the potential to deliver much stronger performance. However, the computation complexity of *SelfAttention3D* grows quadratically with respect to  $\tilde{t} \times \tilde{H} \times \tilde{W}$ , while *SelfAttention1D* is linear with respect to  $\tilde{H}$  and  $\tilde{W}$ , which makes *SelfAttention3D* much more costly at higher resolutions. On the other hand, the computation of *CrossAttentionND* is determined by both spatial-temporal resolution and the number of tokens from the text encoder. *Conv1D* and *3D* are locality alternatives for *SelfAttention1D* and *3D*, respectively. Though the computation complexity and

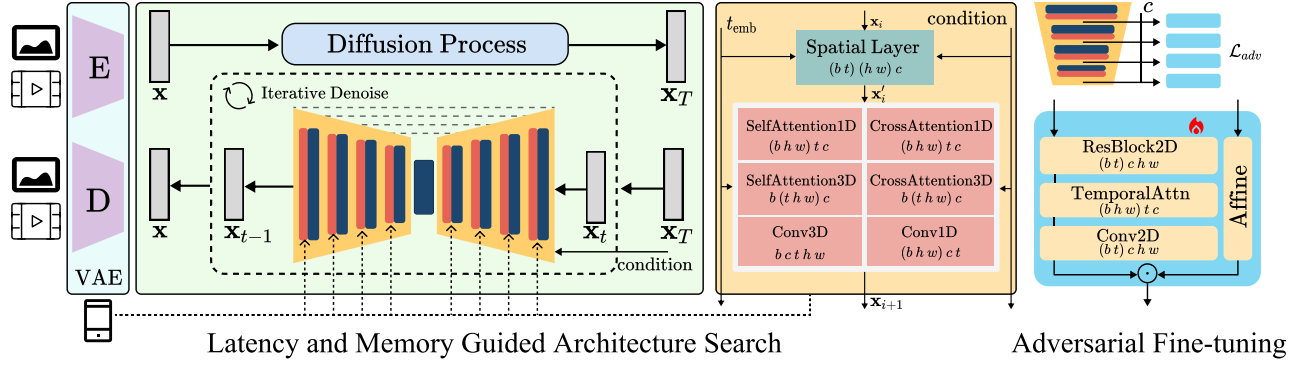


Figure 2. **Framework Overview.** In the Latency and Memory Guided Architecture Search, we freeze the pretrained efficient spatial layers and conduct evolutionary search over temporal layer based on the memory and latency constraint. During the Adversarial Fine-tuning stage, we initialize the discriminator with the weights from the text-to-video model trained in the first stage. The discriminator employs the encoder of the UNet as its backbone, which remains *frozen*. We add spatial-temporal discriminator heads after each downsampling block, updating only these heads during training. Following prior works [48, 49, 74], each head conditions on pooled text embeddings  $\mathbf{c}$  projected via a linear layer. Input features are first reshaped to merge the temporal and batch axes for processing through a 2D ResBlock, and then reshaped again to merge spatial dimensions before the temporal self-attention block.

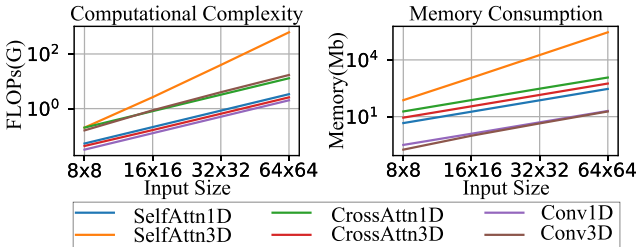


Figure 3. **Computation Complexity and Memory Consumption Analysis.** The computation complexity and memory consumption of different temporal layer for various input size. The temporal dimension is fixed to 12 for simplicity.

memory footprint for each design candidate can be easily profiled, as in Fig. 3, it is still crucial and challenging to build a spatial-temporal network with optimized arrangements of these operators. We propose to perform a latency-memory joint architecture search to determine *which*, *where*, and the *number* of temporal layers to use for our efficient video diffusion model on mobile, as follows.

#### Latency and Memory Guided Architecture Search.

Prior to searching the architecture, we construct a look-up table containing the inference latency and the memory footprint of different temporal layers. For each candidate 1D or 3D operator (*i.e.*, *ConvND*, *SelfAttentionND*, *CrossAttentionND*), we benchmark the latency and memory consumption under different spatial-temporal resolutions on hardware. We then clean the search space by eliminating OOM states. Then we perform evolutionary search to obtain the temporal design with Pareto optimality. The architecture candidate is trained on precomputed video latents for 20K iterations with the spatial backbone frozen, and is evaluated on VBench [19] to obtain the scores as the quality metric.

We include the detailed search algorithm, action space, and total search time in the *supplementary material*.

**Image-Video Joint Training.** Upon the finalized model architecture, we perform image-video joint training under various clip lengths and aspect ratios with all parameters updated for another 100K iterations. After the joint training, our efficient model is capable of generating videos with various lengths and aspect ratios under a conventional recipe, *i.e.*, 25 steps with classifier-free guidance.

**VAE Decoder Compression.** We use the spatial-temporal-decoupled VAE from OpenSora [77], which has 4 latent channels, 8 × 8 spatial compression and 4 × temporal compression. To decode a 17-frame video clip on mobile, the original [77] temporal decoder takes 23,100 ms, and the spatial decoder takes 4100 ms, which we found to be a bottleneck for the generation speed. To increase the speed, we focus on the decoder only. We freeze the VAE encoders and prune the temporal and spatial decoder on our video and image dataset. Our efficient temporal decoder runs at 210 ms and spatial decoder at 330 ms to decode a 17-frame video clip, reaching 50× speedup with negligible loss in quality. Further details about VAE compression are included in the *supplementary material*.

### 3.3. Latent Adversarial Fine-tuning

Our training procedure involves two networks: a generator  $\mathcal{G}_\theta$  and a discriminator  $\mathcal{D}_\phi$ . Similar to prior work [51, 74], we initialize our generator with pre-trained diffusion model weights  $\theta$ , while the discriminator is also partially initialized from  $\theta$ . Specifically, the backbone of the discriminator adopts the same architecture and weights as the pre-trained UNet encoder, with these backbone parameters remaining frozen during training. Additionally, we enhance the dis-

criminator with spatial-temporal discriminator heads added after each backbone block, with only these head parameters being updated in the discriminator training phase. As illustrated on the right in Fig. 2, each discriminator head consists of a spatial ResBlock and a temporal self-attention block. This design allows our discriminator to effectively handle both image and video data during fine-tuning. We analyze the impact of joint image-video fine-tuning in Sec. 4.3.

For a real data sample  $\mathbf{x}_0$ , a noisy data point  $\mathbf{x}_t$  is generated through a forward diffusion process, as described in Eq. (1). We set intermediate timesteps as  $0 < T_k < \dots < T_1 = 1.0$  and sample  $t$  from these timesteps, where  $k$  is the number of timesteps selected for generator training (set to  $k = 4$  in practice). The generator, then, predicts the velocity at  $\mathbf{x}_t$  as  $\mathcal{G}_\theta(\mathbf{x}_t, t)$ .

To train the discriminator, we first sample a target timestep  $t'$  from a logit-normal distribution, as shown in Eq. (3). Using the forward process in Eq. (1), we obtain the real sample  $\mathbf{x}_{t'} = (1 - t')\mathbf{x}_0 + t'\epsilon$ . The fake sample,  $\hat{\mathbf{x}}_{t'}$ , is computed as  $\hat{\mathbf{x}}_{t'} = \mathbf{x}_t + (t' - t) \cdot \mathcal{G}_\theta(t, \mathbf{x}_t)$ , as shown in Fig. 4. Following established approaches [48–50, 74], we employ hinge loss [31] as the adversarial objective to enhance performance. The discriminator’s goal is to differentiate between real and fake samples by minimizing:

$$\begin{aligned} \mathcal{L}_{\text{adv}}^{\mathcal{D}} = & \mathbb{E}_{t', \mathbf{x}_0} [\max(0, 1 + \mathcal{D}_\phi(\mathbf{x}_{t'}, t'))] \\ & + \mathbb{E}_{t, t', \mathbf{x}_0} [\max(0, 1 - \mathcal{D}_\phi(\hat{\mathbf{x}}_{t'}, t'))], \end{aligned} \quad (4)$$

The adversarial objective for the generator is defined as:

$$\mathcal{L}_{\text{adv}}^{\mathcal{G}} = \mathbb{E}_{t, t', \mathbf{x}_0} [\mathcal{D}_\phi(\hat{\mathbf{x}}_{t'}, t')]. \quad (5)$$

Following [74], we also incorporate a reconstruction objective to enhance stability, defined as:

$$\mathcal{L}_{\text{recon}} = \sqrt{\|\hat{\mathbf{x}}_0 - \mathbf{x}_0\|_2^2 + c^2} - c, \quad (6)$$

where  $\hat{\mathbf{x}}_0 = \mathbf{x}_t - t \cdot \mathcal{G}_\theta(t, \mathbf{x}_t)$ , and  $c > 0$  is an adjustable constant.

**Discussion.** Our latent adversarial training pipeline is inspired by SF-V [74]. Similar to SF-V, we set  $k = 4$  and utilize the part of the pre-trained diffusion model as the backbone for the discriminator. However, our approach introduces several key differences. *First*, our method is built on an efficient UNet specifically designed for mobile devices, with fewer parameters than SVD [3], making it a more challenging task. *Second*, we redesign the discriminator heads: instead of using separate spatial and temporal heads, we integrate them into a unified spatial-temporal head for adversarial training. Rather than handling the temporal dimension separately with 1-D convolutional kernels, we incorporate a temporal self-attention layer into the spatial discriminator head after the 2-D ResBlock, forming a spatial-temporal discriminator head. This unified design enables

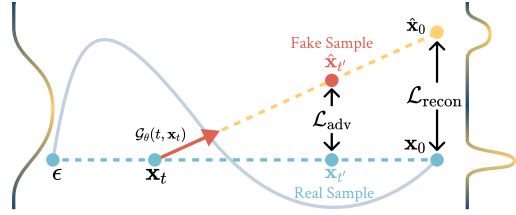


Figure 4. **Latent Adversarial Fine-tuning.** Given a latent  $\mathbf{x}_0$  and a noise latent  $\epsilon$ , we obtain the intermediate noisy latent  $\mathbf{x}_t$  through a forward diffusion process. The generator then predicts the velocity as  $\mathcal{G}_\theta(\mathbf{x}_t, t)$ . Using the predicted velocity, we compute  $\hat{\mathbf{x}}_0$  and calculate the reconstruction loss  $\mathcal{L}_{\text{recon}}$  between  $\mathbf{x}_0$  and  $\hat{\mathbf{x}}_0$ . For adversarial training, the real sample  $\mathbf{x}_{t'}$  is obtained using the same forward diffusion process, while the fake sample  $\hat{\mathbf{x}}_{t'}$  is computed using  $\mathbf{x}_t$  and the predicted velocity  $\mathcal{G}_\theta(\mathbf{x}_t, t)$ .

our model to be jointly trained on both image and video data, which, as demonstrated in Sec. 4.3, significantly enhances the performance of the fine-tuned model.

## 4. Experiments

**Training.** The efficient image backbone is obtained by pruning the Stable Diffusion v1.5 UNet for  $100K$  iterations on high-quality synthetic image datasets. The model is then fine-tuned for  $50K$  additional iterations to adapt to Rectified-Flow velocity prediction [10] as well as to the Spatial-Temporal VAE [77]. We incorporate QK-norm and RoPE [54] in our network to stabilize training. The workflow for architecture search is discussed in Sec. 3.2. The image model pruning, temporal architecture search, and final model training are conducted on 256 NVIDIA A100 80G GPUs using AdamW optimizer with  $5e-5$  learning rate and betas values as  $[0.9, 0.999]$ .

**Adversarial Fine-tuning** is conducted for  $6K$  iterations on 64 NVIDIA A100 GPUs, using the AdamW optimizer with a learning rate of  $1e-7$  for the generator (*i.e.*, UNet) and  $1e-4$  for the discriminator heads. We set the betas as  $[0.9, 0.999]$  for the generator optimizer, and  $[0.5, 0.999]$  for the discriminator optimizer. We set the EMA rate as 0.95 following SF-V [74]. We set  $m = -1, s = 1$  if not otherwise noted.

**Evaluation.** The model is evaluated following the standard benchmarking procedure of VBench [19]. With the 4-step adversarial distilled model, we generate 120-frame horizontal videos at a resolution of  $432 \times 768$  using 4 inference steps without employing classifier-free guidance. The generated video is saved at 5 seconds 24 FPS for score testing and qualitative visualization. The mobile demo and detailed demo settings are included in the *supplementary material*.

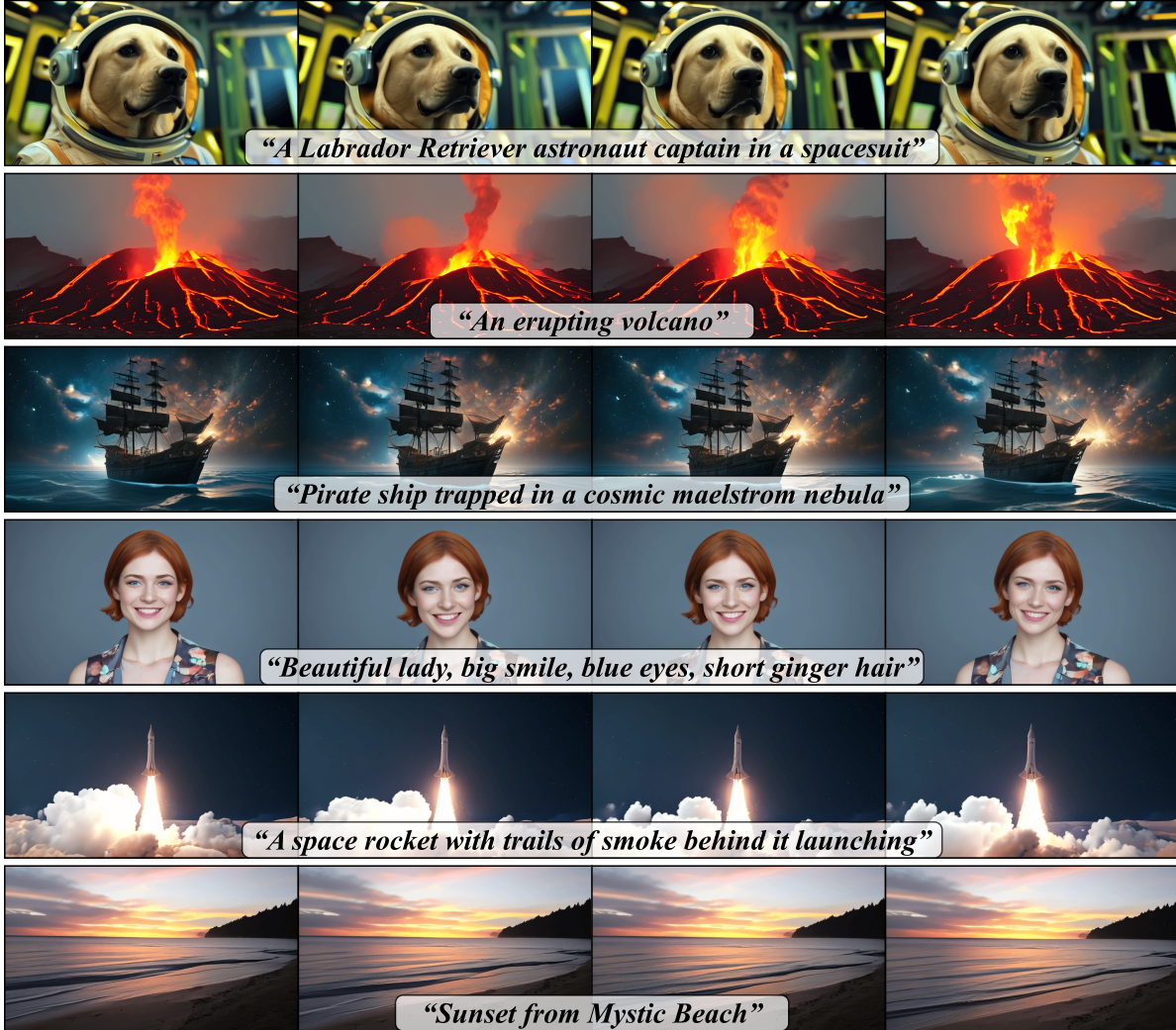


Figure 5. **Video generation on various domains.** We employ our model to synthesize videos across diverse domains, with each video containing 120 frames at a resolution of  $432 \times 768$ . All results are generated through a 4-step inference process. The results demonstrate that our model can produce high-quality, motion-consistent videos featuring various objects across different domains.

Model	Params (B)	Steps	Total score	Quality score	Semantic score	temporal flickering	motion smoothness	dynamic degree	aesthetic quality	object class	multiple objects	color	spatial relationship	appearance style	temporal style	overall consistency
Kling	—	—	81.85	83.39	75.68	99.30	99.40	46.94	61.21	87.24	68.05	89.90	73.03	19.62	24.17	26.42
Pyramid Flow	2.0	20	81.72	84.74	69.62	99.49	99.12	64.63	63.26	86.67	50.71	82.87	59.53	20.91	23.09	26.23
CogVideoX	5.0	50	81.61	82.75	77.04	98.66	96.92	70.97	61.98	85.23	62.11	82.81	66.35	24.91	25.38	27.59
T2V-Turbo	1.6	4	81.01	82.57	74.76	97.48	97.34	49.17	63.04	93.96	54.65	89.90	38.67	24.42	25.51	28.16
Emu3	8.0	—	80.96	84.09	68.43	98.57	98.93	79.27	59.64	86.17	44.64	88.34	68.73	20.92	23.26	24.79
CogVideoX	1.6	50	80.91	82.18	75.83	98.89	97.73	59.86	60.82	83.37	62.63	79.41	69.90	24.80	24.36	26.66
Pika-1.0	—	—	80.69	82.92	71.77	99.74	99.50	47.50	62.04	88.72	43.08	90.57	61.03	22.26	24.22	25.94
VideoCrafter-2.0	1.9	50	80.44	82.20	73.42	98.41	97.73	42.50	63.13	92.55	40.66	92.92	35.86	25.13	25.84	28.23
AnimateDiff-V2	1.2	25	80.27	82.90	69.75	98.75	97.76	40.83	67.16	90.90	36.88	87.47	34.60	22.42	26.03	27.04
OpenSora V1.2	1.2	30	79.76	81.35	73.39	99.53	98.50	42.39	56.85	82.22	51.83	90.08	68.56	23.95	24.54	26.85
AnimateLCM	1.2	4	79.42	82.36	67.65	98.52	98.16	40.56	67.01	91.41	29.76	84.24	37.14	20.97	25.16	26.07
ModelScope	1.4	50	75.75	78.05	66.54	98.28	95.79	66.39	52.06	82.25	38.98	81.72	33.68	23.39	25.37	25.67
Ours	0.6	4	81.14	83.47	71.84	99.37	99.29	51.11	62.19	92.22	54.34	86.63	56.20	20.17	25.18	27.42

Table 2. Performance comparison with popular video generation models on VBench [19].

#### 4.1. Qualitative Visualization

We show visualizations of our generated videos in Fig. 5. Our model consistently produces high-quality video frames and smooth object movements. To demonstrate the generic

text-to-video generation ability, we show various generation examples, including human, animal, photorealistic and art-style scenes. We include more video visualizations in the *supplementary material*.

## 4.2. Quantitative Comparisons

We present a comprehensive evaluation of our method against existing popular video generation models on VBench [19], as in Tab. 2. Despite the fact that our model is compact and designated for fast inference on mobile, it achieves higher total score compared to recent arts, including the DiT-based OpenSora-V1.2, CogVideoX-2B [67], and the UNet-based VideoCrafter-2.0 [6]. In addition, compared to the 4-step distilled T2V-Turbo [27] and AnimateLCM [58], our model achieves better performance with more than 50% reduction in size. The quantitative scores demonstrate the superiority of our efficient model design and the tailored adversarial distillation method.

**User Study.** Human evaluations are conducted between our model and baselines as in the Tab. 3. We generate videos from VBench and Movie Gen Bench prompts and ask human labelers to pick the best results across *prompt alignment*, *aesthetics*, and *motion*. The result shows that our model outperforms baseline metrics by a large margin.

Win Rate	Prompt Alignment	Aesthetics	Motion
OpenSora-1.2	24.9%	21.2%	20.4%
CogVideoX-2B	30.7%	30.5%	30.3%
Ours	44.4%	48.3%	49.3%

Table 3. **User Study** between OpenSora-1.2, CogVideoX-2B, and our model on *prompt alignment*, *aesthetics*, and *motion*.

## 4.3. Ablation Analysis

**Comparison of Training Data Scheme.** We compare the model trained with joint image-video datasets *vs.* video-only datasets. As shown in Tab. 4, training with video-only datasets leads to significant performance degradation on the VBench score with a drop of 6.32 in aesthetic quality, 2.80 in image quality, and 2.54 in total score. The results highlight the importance of joint image-video training, as the image dataset offers more contextual information and enhances diversity.

**Model Scaling.** We scale up and down the model size by adjusting the number of temporal layers, as shown in Tab. 4, to demonstrate the effectiveness of the proposed temporal architecture search. We can observe that scaling up the model can only marginally improve generative scores (*i.e.*,  $\times 2$  scale-up only increasing 0.56 in dynamic degree and 0.12 in motion smoothness, and 0.27 in total score). However, both the  $\times 2$  and  $\times 4$  models hit the memory bound on iPhone. By dividing the  $\times 2$  model into more chunks, we test its mobile speed and observe nearly doubled latency. While on the other hand, further scaling down the model results in heavy losses in generation quality (*i.e.*, decreasing 0.56 in dynamic degree and 0.61 in motion smoothness). Our efficient model is a balanced sweet point for quality and on-device performance.

	w/I Scaling	$\Delta T$	$\Delta AQ$	$\Delta IQ$	$\Delta DD$	$\Delta MS$	$\Delta Total$
Video-only	$\times$	—	—	-6.32	-2.80	+4.6	-0.17
Temporal Scaling	$\checkmark$	$\times 0.5$	-22%	-1.90	+0.04	-0.56	-0.61
		$\times 2$	+32%	+0.37	+0.10	+0.56	+0.12
		$\times 4$	+107%	+0.49	-0.17	+0.91	+0.17

Table 4. **Analysis of training data scheme, latency, and quality of efficient architecture.** The baseline model adopts the best suitable architecture and is trained with joint image-video datasets. The “scaling”, and “T” indicates the number of the temporal layers, and the latency comparing to the baseline. The “AQ”, “IQ”, “DD”, and “MS”, are aesthetic quality, image quality, dynamic degree, and motion smoothness in VBench [19]. The benchmark metrics are presented as the differences from the baseline model, where negative values indicates a decrease in performance over the baseline vice versa.

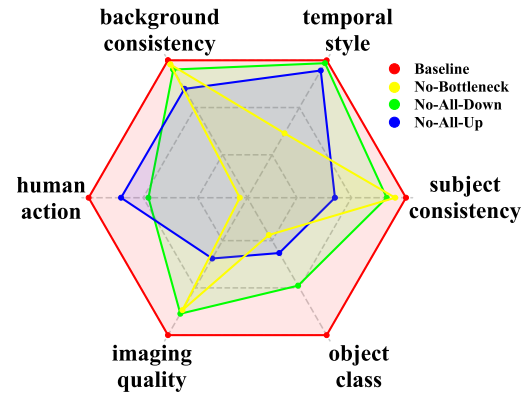


Figure 6. **Analysis of temporal layers.** We ablate temporal layers in different network stages to evaluate their effect. The scores are normalized according to our base model to better demonstrate the difference.

**Effect of Different Temporal Layers.** To better understand the roles of the searched temporal layers, we compute the VBench score after systematically removing (i) all temporal layers in the downsample stage, (ii) bottleneck temporal layers, and (iii) all temporal layers in the upsample stage. The model makes reasonable zero-shot generations after temporal layer removal, but we still fine-tune 10K iterations under the same recipe as in Sec. 3.2 for fair comparison. As shown in Fig. 6, removing different temporal layers results in varying degrees of performance degradation across different metrics, and all removing strategies result in a substantial drop in total score, demonstrating that the existence of the searched temporal layers is important, and they play different roles in generation. Specifically, removing temporal layers in upsample blocks results in a more significant loss in imaging quality, subject consistency, and background consistency, suggesting that the up temporal layers play important roles in detail reconstruction. In contrast, bottleneck layers are more important in human action and object class, where global information modeling dom-

inates the results. We observe that removing down layers introduces less overall degradations compared to the other two, which is an anticipated phenomenon because the loss of modeling capacity can be mitigated by the subsequent bottleneck and up stage temporal layers after fine-tuning.

Head	w/I	w/ $\mathcal{L}_{\text{adv}}$	$m$	TF	MO	Q	S	Total
SF-V [74]	$\times$	$\checkmark$	-1	98.86	30.75	83.60	64.25	79.73
Ours	$\checkmark$	$\times$	-1	99.27	37.85	83.61	69.01	80.69
Ours	$\checkmark$	$\checkmark$	-1	97.32	1.01	70.03	17.04	59.44
			-2	99.29	47.64	83.91	70.54	81.23
Ours	$\checkmark$	$\checkmark$	-1	99.37	54.34	83.47	71.84	81.14
			0	99.44	43.63	81.69	69.46	79.24
			1	99.56	24.41	77.84	58.88	74.05

**Table 5. Analysis of our adversarial fine-tuning scheme.** We evaluate the VBench [19] scores for our models using different training schemes. In the results, “TF” and “MO” denote the temporal flickering and multiple objects sub-scores, respectively, while “Q” and “S” represent the quality and semantic scores. The table summarizes how varying (1) the type of discriminator head, (2) training with or without an image dataset, and (3) different  $t'$  distributions impact the performance of our model.

**Effect of Discriminator Heads.** We compare the effects of our spatial-temporal discriminator heads with the separate spatial and temporal heads proposed in SF-V [74] to demonstrate the effectiveness of our discriminator architecture. For a fair comparison, both models are trained exclusively on video data. We evaluate the models fine-tuned with different discriminator heads on VBench [19]. As shown in the first two rows of Tab. 5, our discriminator heads result in improvements in both the quality score (83.61 *vs.* 83.60) and the semantic score (69.01 *vs.* 64.25) of the generated videos.

**Effect of Joint Image Video Fine-tuning.** We examine the impact of incorporating image data during adversarial training, as shown in the second and fourth rows of Tab. 5. The results indicate that fine-tuning the model with image data can slightly decrease the Quality score in the VBench [19] evaluation (from 83.61 to 83.47). However, by leveraging the increased diversity of the image dataset, the model achieves a substantial improvement in semantic performance, particularly in multi-object generation (from 37.85 to 54.34). This enhancement leads to a better overall score compared to the model trained exclusively on video data (81.14 *vs.* 80.69).

**Effect of Noise Distribution for Discriminator.** Following Eq. (3), the parameters  $m$  and  $s$  control the distribution of  $t'$ , which determines the noise levels of  $\mathbf{x}_{t'}$  and  $\hat{\mathbf{x}}_{t'}$  before they are passed to the discriminator as real and fake samples, respectively. We investigate the effect of different noise distributions on model performance by evaluating the results using VBench [19]. As shown in the last four rows of Tab. 5, increasing  $m$  (resulting in noisier real and fake sam-

ples) degrades the quality score (from 83.91 to 77.84) while slightly enhancing the temporal flickering score (from 99.29 to 99.56). Although setting  $m = -2$  achieves the highest overall score among the experiments (81.23), it performs poorly on multi-object generation. Therefore, in most of our experiments, unless otherwise stated, we use  $m = -1$ . This setting yields a slightly lower overall score (81.14) but significantly improves semantic performance (71.84 *vs.* 70.54) and excels in multi-object generation (54.34 *vs.* 47.64).

# Steps	DD	OC	AQ	Quality	Semantic	Total
1	11.39	79.24	52.85	74.43	62.70	72.09
2	30.28	88.97	59.74	80.08	69.28	77.92
4	51.11	92.22	62.19	83.47	71.84	81.14

**Table 6. Analysis of the number of inference steps.** We measure VBench [19] score with different numbers of inference steps. In the results, “DD”, “OC”, and “AQ” denote the dynamic degree, object class, and aesthetic quality scores, respectively.

**Effect of Inference Steps.** Our fine-tuned model supports generation with a reduced number of inference steps. We further investigate how varying the number of evaluation steps affects the quality of the generated results, as shown in Tab. 6. While our four-step generation achieves the best performance, even with only two steps, the model still produces reasonable results. Increasing the number of inference steps improves the performance of our model across all metrics. In Tab. 6, we report not only the quality and semantic scores but also scores for dynamic degree, object class, and aesthetic quality. However, reducing the process to a single inference step leads to a significant drop in performance. We leave more aggressive step reductions to future work.

## 5. Discussion and Conclusion

In this work, we propose an acceleration framework for the video diffusion model, and for the first time, achieve super-fast text-to-video generation on mobile devices. Specifically, we discover an efficient but powerful network architecture through latency and memory joint architecture search for temporal layers. In addition, we propose an improved adversarial fine-tuning technique to distill our model to 4 steps to further speed up generation. Our work is a good starting point for the edge deployment of video diffusion models and we hope to inspire more downstream applications such as video extension and editing.

**Limitations.** We use a public 4-channel VAE [77] to encode videos to latent space. Recent work has shown that using more latent channels benefits reconstruction details. Another future direction is to further improve the step reduction technique for 1-2 denoising steps, as works [74] on server-level models.

## References

[1] Luma AI. Dream machine. <https://lumalabs.ai/dream-machine>, . 2

[2] Pika AI. Pika 1.5. <https://pika.art/try>, . 2

[3] Andreas Blattmann, Tim Dockhorn, Sumith Kulal, Daniel Mendelevitch, Maciej Kilian, Dominik Lorenz, Yam Levi, Zion English, Vikram Voleti, Adam Letts, et al. Stable video diffusion: Scaling latent video diffusion models to large datasets. *ArXiv preprint*, abs/2311.15127, 2023. 1, 2, 3, 5

[4] Andreas Blattmann, Robin Rombach, Huan Ling, Tim Dockhorn, Seung Wook Kim, Sanja Fidler, and Karsten Kreis. Align your latents: High-resolution video synthesis with latent diffusion models. In *IEEE/CVF Conference on Computer Vision and Pattern Recognition, CVPR 2023, Vancouver, BC, Canada, June 17-24, 2023*, pages 22563–22575. IEEE, 2023. 1, 2

[5] Haoxin Chen, Menghan Xia, Yingqing He, Yong Zhang, Xiaodong Cun, Shaoshu Yang, Jinbo Xing, Yaofang Liu, Qifeng Chen, Xintao Wang, et al. Videocrafter1: Open diffusion models for high-quality video generation. *ArXiv preprint*, abs/2310.19512, 2023. 2

[6] Haoxin Chen, Yong Zhang, Xiaodong Cun, Menghan Xia, Xintao Wang, Chao Weng, and Ying Shan. Videocrafter2: Overcoming data limitations for high-quality video diffusion models. In *Proceedings of the IEEE/CVF Conference on Computer Vision and Pattern Recognition*, pages 7310–7320, 2024. 2, 7

[7] Tsai-Shien Chen, Aliaksandr Siarohin, Willi Menapace, Ekaterina Deyneka, Hsiang-wei Chao, Byung Eun Jeon, Yuwei Fang, Hsin-Ying Lee, Jian Ren, Ming-Hsuan Yang, et al. Panda-70m: Captioning 70m videos with multiple cross-modality teachers. In *Proceedings of the IEEE/CVF Conference on Computer Vision and Pattern Recognition*, pages 13320–13331, 2024. 2

[8] Xinwang Chen, Ning Liu, Yichen Zhu, Feifei Feng, and Jian Tang. Edt: An efficient diffusion transformer framework inspired by human-like sketching. *ArXiv preprint*, abs/2410.23788, 2024. 1, 2

[9] Trung Dao, Thuan Hoang Nguyen, Thanh Le, Duc Vu, Khoi Nguyen, Cuong Pham, and Anh Tran. Swiftbrush v2: Make your one-step diffusion model better than its teacher. In *European Conference on Computer Vision*, pages 176–192. Springer, 2025. 3

[10] Patrick Esser, Sumith Kulal, Andreas Blattmann, Rahim Entezari, Jonas Müller, Harry Saini, Yam Levi, Dominik Lorenz, Axel Sauer, Frederic Boesel, et al. Scaling rectified flow transformers for high-resolution image synthesis. In *Forty-first International Conference on Machine Learning*, 2024. 3, 5

[11] Gongfan Fang, Xinyin Ma, and Xinchao Wang. Structural pruning for diffusion models. In *Advances in Neural Information Processing Systems 36: Annual Conference on Neural Information Processing Systems 2023, NeurIPS 2023, New Orleans, LA, USA, December 10 - 16, 2023*, 2023. 2, 3

[12] Yutang Feng, Sicheng Gao, Yuxiang Bao, Xiaodi Wang, Shumin Han, Juan Zhang, Baochang Zhang, and Angela Yao. Wave: Warping ddim inversion features for zero-shot text-to-video editing. In *European Conference on Computer Vision*, pages 38–55. Springer, 2025. 1

[13] Yuwei Guo, Ceyuan Yang, Anyi Rao, Zhengyang Liang, Yaohui Wang, Yu Qiao, Maneesh Agrawala, Dahua Lin, and Bo Dai. Animatediff: Animate your personalized text-to-image diffusion models without specific tuning. *ArXiv preprint*, abs/2307.04725, 2023. 1, 2, 3

[14] Yuwei Guo, Ceyuan Yang, Anyi Rao, Maneesh Agrawala, Dahua Lin, and Bo Dai. Sparsectrl: Adding sparse controls to text-to-video diffusion models. In *European Conference on Computer Vision*, pages 330–348. Springer, 2025. 2

[15] Agrim Gupta, Lijun Yu, Kihyuk Sohn, Xiuye Gu, Meera Hahn, Li Fei-Fei, Irfan Essa, Lu Jiang, and José Lezama. Photorealistic video generation with diffusion models. *ArXiv preprint*, abs/2312.06662, 2023. 2

[16] Jonathan Ho and Tim Salimans. Classifier-free diffusion guidance. *ArXiv preprint*, abs/2207.12598, 2022. 2

[17] Jonathan Ho, Ajay Jain, and Pieter Abbeel. Denoising diffusion probabilistic models. In *Advances in Neural Information Processing Systems 33: Annual Conference on Neural Information Processing Systems 2020, NeurIPS 2020, December 6-12, 2020, virtual*, 2020. 2, 3

[18] Wenyi Hong, Ming Ding, Wendi Zheng, Xinghan Liu, and Jie Tang. Cogvideo: Large-scale pretraining for text-to-video generation via transformers. In *The Eleventh International Conference on Learning Representations, ICLR 2023, Kigali, Rwanda, May 1-5, 2023*. OpenReview.net, 2023. 2

[19] Ziqi Huang, Yinan He, Jiashuo Yu, Fan Zhang, Chenyang Si, Yuming Jiang, Yuanhan Zhang, Tianxing Wu, Qingyang Jin, Nattapol Chanpaisit, Yaohui Wang, Xinyuan Chen, Limin Wang, Dahua Lin, Yu Qiao, and Ziwei Liu. Vbench: Comprehensive benchmark suite for video generative models. In *Proceedings of the IEEE/CVF Conference on Computer Vision and Pattern Recognition*, 2024. 2, 4, 5, 6, 7, 8, 1

[20] Hyeonho Jeong, Jinho Chang, Geon Yeong Park, and Jong Chul Ye. Dreammotion: Space-time self-similar score distillation for zero-shot video editing. *ArXiv preprint*, abs/2403.12002, 2024. 1

[21] Yang Jin, Zhicheng Sun, Ningyuan Li, Kun Xu, Hao Jiang, Nan Zhuang, Quzhe Huang, Yang Song, Yadong Mu, and Zhouchen Lin. Pyramidal flow matching for efficient video generative modeling. *ArXiv preprint*, abs/2410.05954, 2024. 2

[22] Beomsu Kim, Yu-Guan Hsieh, Michal Klein, Marco Cuturi, Jong Chul Ye, Bahjat Kawar, and James Thornton. Simple reflow: Improved techniques for fast flow models. *ArXiv preprint*, abs/2410.07815, 2024. 3

[23] Jihwan Kim, Junoh Kang, Jinyoung Choi, and Bohyung Han. Fifo-diffusion: Generating infinite videos from text without training. *ArXiv preprint*, abs/2405.11473, 2024. 2

[24] Kuaishou. Kling. <https://kling.kuaishou.com/en>. 2

[25] Jeong-gi Kwak, Erqun Dong, Yuhe Jin, Hanseok Ko, Shweta Mahajan, and Kwang Moo Yi. Vivid-1-to-3: Novel view synthesis with video diffusion models. In *Proceedings of the IEEE/CVF Conference on Computer Vision and Pattern Recognition*, pages 6775–6785, 2024. 1

[26] PKU-Yuan Lab and Tuzhan AI etc. Open-sora-plan, 2024. 2

[27] Jiachen Li, Weixi Feng, Tsu-Jui Fu, Xinyi Wang, Sugato Basu, Wenhui Chen, and William Yang Wang. T2v-turbo: Breaking the quality bottleneck of video consistency model with mixed reward feedback. *ArXiv preprint*, abs/2405.18750, 2024. 2, 7

[28] Jiachen Li, Qian Long, Jian Zheng, Xiaofeng Gao, Robinson Piramuthu, Wenhui Chen, and William Yang Wang. T2v-turbo-v2: Enhancing video generation model post-training through data, reward, and conditional guidance design. *ArXiv preprint*, abs/2410.05677, 2024. 2

[29] Yanyu Li, Huan Wang, Qing Jin, Ju Hu, Pavlo Chemerys, Yun Fu, Yanzhi Wang, Sergey Tulyakov, and Jian Ren. Snap-fusion: Text-to-image diffusion model on mobile devices within two seconds. In *Advances in Neural Information Processing Systems 36: Annual Conference on Neural Information Processing Systems 2023, NeurIPS 2023, New Orleans, LA, USA, December 10 - 16, 2023*, 2023. 2, 3

[30] Feng Liang, Bichen Wu, Jialiang Wang, Licheng Yu, Kunpeng Li, Yinan Zhao, Ishan Misra, Jia-Bin Huang, Peizhao Zhang, Peter Vajda, et al. Flowvid: Taming imperfect optical flows for consistent video-to-video synthesis. In *Proceedings of the IEEE/CVF Conference on Computer Vision and Pattern Recognition*, pages 8207–8216, 2024. 1

[31] Jae Hyun Lim and Jong Chul Ye. Geometric gan. *ArXiv preprint*, abs/1705.02894, 2017. 5

[32] Shanchuan Lin and Xiao Yang. Animatediff-lightning: Cross-model diffusion distillation. *ArXiv preprint*, abs/2403.12706, 2024. 3

[33] Xingchao Liu, Chengyue Gong, and Qiang Liu. Flow straight and fast: Learning to generate and transfer data with rectified flow. In *The Eleventh International Conference on Learning Representations, ICLR 2023, Kigali, Rwanda, May 1-5, 2023*. OpenReview.net, 2023. 3

[34] Yu Lu, Yuanzhi Liang, Linchao Zhu, and Yi Yang. Free-long: Training-free long video generation with spectralblend temporal attention. *ArXiv preprint*, abs/2407.19918, 2024. 2

[35] Xiaofeng Mao, Zhengkai Jiang, Fu-Yun Wang, Wenbing Zhu, Jiangning Zhang, Hao Chen, Mingmin Chi, and Yabiao Wang. Osv: One step is enough for high-quality image to video generation. *ArXiv preprint*, abs/2409.11367, 2024. 3

[36] Kangfu Mei, Mauricio Delbracio, Hossein Talebi, Zhengzhong Tu, Vishal M Patel, and Peyman Milanfar. Codi: Conditional diffusion distillation for higher-fidelity and faster image generation. In *Proceedings of the IEEE/CVF Conference on Computer Vision and Pattern Recognition*, pages 9048–9058, 2024. 3

[37] MiniMax. Hailuo ai. <https://hailuoai.video/>. 2

[38] Kepan Nan, Rui Xie, Penghao Zhou, Tiehan Fan, Zhenheng Yang, Zhijie Chen, Xiang Li, Jian Yang, and Ying Tai. Openvid-1m: A large-scale high-quality dataset for text-to-video generation. *ArXiv preprint*, abs/2407.02371, 2024. 2

[39] OpenAI. Video generation models as world simulators. <https://openai.com/index/video-generation-models-as-world-simulators/>. 2

[40] William Peebles and Saining Xie. Scalable diffusion models with transformers. In *IEEE/CVF International Conference on Computer Vision, ICCV 2023, Paris, France, October 1-6, 2023*, pages 4172–4182. IEEE, 2023. 1, 2, 3

[41] Adam Polyak, Amit Zohar, Andrew Brown, Andros Tjandra, Animesh Sinha, Ann Lee, Apoorv Vyas, Bowen Shi, Chih-Yao Ma, Ching-Yao Chuang, et al. Movie gen: A cast of media foundation models. *ArXiv preprint*, abs/2410.13720, 2024. 1, 2

[42] Zhiwu Qing, Shiwei Zhang, Jiayu Wang, Xiang Wang, Yujie Wei, Yingya Zhang, Changxin Gao, and Nong Sang. Hierarchical spatio-temporal decoupling for text-to-video generation. In *Proceedings of the IEEE/CVF Conference on Computer Vision and Pattern Recognition*, pages 6635–6645, 2024. 2

[43] Haonan Qiu, Menghan Xia, Yong Zhang, Yingqing He, Xintao Wang, Ying Shan, and Ziwei Liu. Freenoise: Tuning-free longer video diffusion via noise rescheduling. *ArXiv preprint*, abs/2310.15169, 2023. 2

[44] Yixuan Ren, Yang Zhou, Jimei Yang, Jing Shi, Difan Liu, Feng Liu, Mingi Kwon, and Abhinav Shrivastava. Customize-a-video: One-shot motion customization of text-to-video diffusion models. *ArXiv preprint*, abs/2402.14780, 2024. 2

[45] Robin Rombach, Andreas Blattmann, Dominik Lorenz, Patrick Esser, and Björn Ommer. High-resolution image synthesis with latent diffusion models. In *Proceedings of the IEEE/CVF conference on computer vision and pattern recognition*, pages 10684–10695, 2022. 1, 2, 3

[46] Runway. Gen-3 alpha. <https://runwayml.com/research/introducing-gen-3-alpha>. 2

[47] Tim Salimans and Jonathan Ho. Progressive distillation for fast sampling of diffusion models. In *The Tenth International Conference on Learning Representations, ICLR 2022, Virtual Event, April 25-29, 2022*. OpenReview.net, 2022. 3

[48] Axel Sauer, Kashyap Chitta, Jens Müller, and Andreas Geiger. Projected gans converge faster. In *Advances in Neural Information Processing Systems 34: Annual Conference on Neural Information Processing Systems 2021, NeurIPS 2021, December 6-14, 2021, virtual*, pages 17480–17492, 2021. 4, 5

[49] Axel Sauer, Tero Karras, Samuli Laine, Andreas Geiger, and Timo Aila. Stylegan-t: Unlocking the power of gans for fast large-scale text-to-image synthesis. In *International Conference on Machine Learning, ICML 2023, 23-29 July 2023, Honolulu, Hawaii, USA*, pages 30105–30118. PMLR, 2023. 4

[50] Axel Sauer, Dominik Lorenz, Andreas Blattmann, and Robin Rombach. Adversarial diffusion distillation. *ArXiv preprint*, abs/2311.17042, 2023. 3, 5

[51] Axel Sauer, Frederic Boesel, Tim Dockhorn, Andreas Blattmann, Patrick Esser, and Robin Rombach. Fast high-resolution image synthesis with latent adversarial diffusion distillation. *ArXiv preprint*, abs/2403.12015, 2024. 3, 4

[52] Yang Song and Prafulla Dhariwal. Improved techniques for training consistency models. *ArXiv preprint*, abs/2310.14189, 2023. 3

[53] Yang Song, Prafulla Dhariwal, Mark Chen, and Ilya Sutskever. Consistency models. In *International Conference on Machine Learning, ICML 2023, 23-29 July 2023*, 2023. 3

*Honolulu, Hawaii, USA*, pages 32211–32252. PMLR, 2023. 3

[54] Jianlin Su, Murtadha Ahmed, Yu Lu, Shengfeng Pan, Wen Bo, and Yunfeng Liu. Roformer: Enhanced transformer with rotary position embedding. *Neurocomputing*, 568:127063, 2024. 5

[55] Genmo Team. Mochi, 2024. 1, 2

[56] Gemini Team, Rohan Anil, Sebastian Borgeaud, Jean-Baptiste Alayrac, Jiahui Yu, Radu Soricut, Johan Schalkwyk, Andrew M Dai, Anja Hauth, Katie Millican, et al. Gemini: a family of highly capable multimodal models. *ArXiv preprint*, abs/2312.11805, 2023. 1, 2

[57] Vikram Voleti, Chun-Han Yao, Mark Boss, Adam Letts, David Pankratz, Dmitry Tochilkin, Christian Laforet, Robin Rombach, and Varun Jampani. Sv3d: Novel multi-view synthesis and 3d generation from a single image using latent video diffusion. In *European Conference on Computer Vision*, pages 439–457. Springer, 2025. 1

[58] Fu-Yun Wang, Zhaoyang Huang, Xiaoyu Shi, Weikang Bian, Guanglu Song, Yu Liu, and Hongsheng Li. Animateclm: Accelerating the animation of personalized diffusion models and adapters with decoupled consistency learning. *ArXiv preprint*, abs/2402.00769, 2024. 3, 7

[59] Fu-Yun Wang, Ling Yang, Zhaoyang Huang, Mengdi Wang, and Hongsheng Li. Rectified diffusion: Straightness is not your need in rectified flow. *ArXiv preprint*, abs/2410.07303, 2024. 3

[60] Xiang Wang, Shiwei Zhang, Han Zhang, Yu Liu, Yingya Zhang, Changxin Gao, and Nong Sang. Videolcm: Video latent consistency model. *ArXiv preprint*, abs/2312.09109, 2023. 3

[61] Jianzong Wu, Xiangtai Li, Yanhong Zeng, Jiangning Zhang, Qianyu Zhou, Yining Li, Yunhai Tong, and Kai Chen. Motionbooth: Motion-aware customized text-to-video generation. *ArXiv preprint*, abs/2406.17758, 2024. 2

[62] Jay Zhangjie Wu, Yixiao Ge, Xintao Wang, Stan Weixian Lei, Yuchao Gu, Yufei Shi, Wynne Hsu, Ying Shan, Xiaohu Qie, and Mike Zheng Shou. Tune-a-video: One-shot tuning of image diffusion models for text-to-video generation. In *IEEE/CVF International Conference on Computer Vision, ICCV 2023, Paris, France, October 1-6, 2023*, pages 7589–7599. IEEE, 2023. 1, 2

[63] Tianxing Wu, Chenyang Si, Yuming Jiang, Ziqi Huang, and Ziwei Liu. Freeinit: Bridging initialization gap in video diffusion models. In *European Conference on Computer Vision*, pages 378–394. Springer, 2025. 2

[64] Enze Xie, Junsong Chen, Junyu Chen, Han Cai, Yujun Lin, Zhekai Zhang, Muyang Li, Yao Lu, and Song Han. Sana: Efficient high-resolution image synthesis with linear diffusion transformers. *ArXiv preprint*, abs/2410.10629, 2024. 1

[65] Yanwu Xu, Yang Zhao, Zhisheng Xiao, and Tingbo Hou. Ufogen: You forward once large scale text-to-image generation via diffusion gans. In *Proceedings of the IEEE/CVF Conference on Computer Vision and Pattern Recognition*, pages 8196–8206, 2024. 3

[66] Ling Yang, Zixiang Zhang, Zhilong Zhang, Xingchao Liu, Minkai Xu, Wentao Zhang, Chenlin Meng, Stefano Ermon, and Bin Cui. Consistency flow matching: Defining straight flows with velocity consistency. *ArXiv preprint*, abs/2407.02398, 2024. 3

[67] Zhuoyi Yang, Jiayan Teng, Wendi Zheng, Ming Ding, Shiyu Huang, Jiazheng Xu, Yuanming Yang, Wenyi Hong, Xiaohan Zhang, Guanyu Feng, et al. Cogvideox: Text-to-video diffusion models with an expert transformer. *ArXiv preprint*, abs/2408.06072, 2024. 1, 2, 3, 7, 5

[68] Tianwei Yin, Michaël Gharbi, Taesung Park, Richard Zhang, Eli Shechtman, Fredo Durand, and William T Freeman. Improved distribution matching distillation for fast image synthesis. *ArXiv preprint*, abs/2405.14867, 2024. 3

[69] Tianwei Yin, Michaël Gharbi, Richard Zhang, Eli Shechtman, Fredo Durand, William T Freeman, and Taesung Park. One-step diffusion with distribution matching distillation. In *Proceedings of the IEEE/CVF Conference on Computer Vision and Pattern Recognition*, pages 6613–6623, 2024. 3

[70] Zhihang Yuan, Pu Lu, Hanling Zhang, Xuefei Ning, Linfeng Zhang, Tianchen Zhao, Shengen Yan, Guohao Dai, and Yu Wang. Diffastattn: Attention compression for diffusion transformer models. *ArXiv preprint*, abs/2406.08552, 2024. 1, 2

[71] Yan Zeng, Guoqiang Wei, Jiani Zheng, Jiaxin Zou, Yang Wei, Yuchen Zhang, and Hang Li. Make pixels dance: High-dynamic video generation. In *Proceedings of the IEEE/CVF Conference on Computer Vision and Pattern Recognition*, pages 8850–8860, 2024. 2

[72] Yuanhao Zhai, Kevin Lin, Zhengyuan Yang, Linjie Li, Jianfeng Wang, Chung-Ching Lin, David Doermann, Junsong Yuan, and Lijuan Wang. Motion consistency model: Accelerating video diffusion with disentangled motion-appearance distillation. *ArXiv preprint*, abs/2406.06890, 2024. 3

[73] Zheng Zhan, Yushu Wu, Yifan Gong, Zichong Meng, Zhenglun Kong, Changdi Yang, Geng Yuan, Pu Zhao, Wei Niu, and Yanzhi Wang. Fast and memory-efficient video diffusion using streamlined inference. In *The Thirty-eighth Annual Conference on Neural Information Processing Systems*. 2

[74] Zhixing Zhang, Yanyu Li, Yushu Wu, Yanwu Xu, Anil Kag, Ivan Skorokhodov, Willi Menapace, Aliaksandr Siarohin, Junli Cao, Dimitris Metaxas, et al. Sf-v: Single forward video generation model. *ArXiv preprint*, abs/2406.04324, 2024. 3, 4, 5, 8

[75] Zhixing Zhang, Bichen Wu, Xiaoyan Wang, Yaqiao Luo, Luxin Zhang, Yinan Zhao, Peter Vajda, Dimitris Metaxas, and Licheng Yu. Avid: Any-length video inpainting with diffusion model. In *Proceedings of the IEEE/CVF Conference on Computer Vision and Pattern Recognition*, pages 7162–7172, 2024. 2

[76] Rui Zhao, Yuchao Gu, Jay Zhangjie Wu, David Junhao Zhang, Jia-Wei Liu, Weijia Wu, Jussi Keppo, and Mike Zheng Shou. Motiondirector: Motion customization of text-to-video diffusion models. In *European Conference on Computer Vision*, pages 273–290. Springer, 2025. 2

[77] Zangwei Zheng, Xiangyu Peng, Tianji Yang, Chenhui Shen, Shenggui Li, Hongxin Liu, Yukun Zhou, Tianyi Li, and Yang You. Open-sora: Democratizing efficient video production for all, 2024. 2, 3, 4, 5, 8, 1

- [78] Yuan Zhou, Qiuyue Wang, Yuxuan Cai, and Huan Yang. Allegro: Open the black box of commercial-level video generation model. *ArXiv preprint*, abs/2410.15458, 2024. [1](#), [2](#)
- [79] Yupeng Zhou, Daquan Zhou, Ming-Ming Cheng, Jiashi Feng, and Qibin Hou. Storydiffusion: Consistent self-attention for long-range image and video generation. *NeurIPS 2024*, 2024. [2](#)

# SnapGen-V: Generating a Five-Second Video within Five Seconds on a Mobile Device

## Supplementary Material

### Overview

The supplementary material accompanying this paper provides additional insights and elaborations on various aspects of our proposed method. The contents are organized as follows:

- **Search Algorithm:** Appendix A provides a detailed search algorithm we proposed to determine the final architecture of our model.
- **VAE Compression:** Appendix B describes the separable efficient variational autoencoder we employed for efficient video generation on mobile devices.
- **Qualitative and Quantitative Results for the Spatial Backbone:** We showcase a broad range of qualitative results demonstrating the effectiveness of our spatial backbone. The quantitative results is also evaluated. The results can be found in Appendix C.
- **Qualitative Comparison Results:** The qualitative comparison of our model with two popular open-source models (OponSora-v1.2 [77] and CogVideoX-2B [67]) is shown in Appendix D. More results can be found in the *accompanying webpage*.
- **More Qualitative Results:** Additional qualitative results are presented in Appendix E. We also provide these results in video format in the *accompanying webpage*.
- **Demo:** We provide our demo benchmark and mobile screenshots in Appendix F.
- **Effect of Adversarial Fine-tuning:** We further discuss the effect of adversarial finetuning for step distillation in Appendix G.
- **Latency Analysis:** Appendix H shows the latency analysis of different temporal blocks.

### A. Search Algorithm

We propose a two-step architecture search to design temporal layers that satisfy hardware constraints and performance requirements. First, a coarse architecture search is conducted based on the spatial backbone, eliminating candidate architectures that violate the hardware constraints to narrow the search space. Then, we build an action set,  $\mathcal{A} \in \{A_{SelfAttnND[i]}^{+,-}, A_{CrossAttnND[i]}^{+,-}, A_{ConvND[i]}^{+,-}\}$ , to perform the evolutionary search, where the  $A^{+,-}$  indicates the action to add or remove the temporal layer for corresponding position ( $i^{th}$  block). The action is guided by latency and memory constraints, as well as generation performance. We choose the Vbench score [19] to evaluate the quantitative performance of each architecture, and we specifically

focus on the average score of the *overall consistency*, the *object class*, and the *color* score instead of the complete benchmark to reduce the evaluation time. The value score of each action is defined as  $\{\frac{\Delta V_{bench}}{\Delta Latency}, \frac{\Delta V_{bench}}{\Delta Memory}\}$ . We use 268 prompts with 25 denoising steps and 7 classifier-free guidance scale to benchmark those scores above in Vbench [19], and it takes 8 A100 GPU hours to evaluate each action. We further simplify the search space by avoiding a mixture of temporal layers in the same position. As shown in Algorithm A1, different temporal layers are integrated into the UNet at each search step, with evaluations based on the selected Vbench score after training the model for 20K iterations. The latency and peak memory are retrieved from the pre-built look-up table. The action is then updated based on the  $\frac{\Delta V_{bench}}{\Delta Latency}$  and  $\frac{\Delta V_{bench}}{\Delta Memory}$ , prioritizing temporal layers that offer low latency and memory consumption while contributing more significantly to a better Vbench score.

---

#### Algorithm A1 Search Algorithm

---

**Require:**

UNet:  $\hat{\epsilon}_\theta$ ;  
validation set:  $\mathbb{D}_{val}$ ;  
latency and memory lookup table  $\mathbb{T}$  :  
 $\{SelfAttnND[i], CrossAttnND[i], ConvND[i]\}$ .

**Ensure:**  $\hat{\epsilon}_\theta$  converges and satisfies latency objective  $S$ .

**while**  $\hat{\epsilon}_\theta$  not converged **do**

→ **Architecture optimization:**

if perform architecture evolving at this iteration **then**

→ **Evaluate blocks:**

for each block $[i]$  **do**

$\Delta V_{bench} \leftarrow \text{eval}(\hat{\epsilon}_\theta, A_{block[i]}^-, \mathbb{D}_{val})$ ,

$\Delta Latency, \Delta Memory \leftarrow \text{eval}(\hat{\epsilon}_\theta, A_{block[i]}^-, \mathbb{T})$

**end for**

→ **Sort actions based on  $\frac{\Delta V_{bench}}{\Delta Latency}$  and  $\frac{\Delta V_{bench}}{\Delta Memory}$** , execute action, and evolve architecture to get latency  $T$  and peak memory  $M$ :

if  $T$  not satisfied **then**

$\{\hat{A}^-\} \leftarrow \arg \min_{A^-} \frac{\Delta V_{bench}}{\Delta Latency}$ ,

else if  $M$  not satisfied **then**

$\{\hat{A}^-\} \leftarrow \arg \min_{A^-} \frac{\Delta V_{bench}}{\Delta Memory}$ ,

else

$\{\hat{A}^+\} \leftarrow \text{add}(\arg \max_{A^+} \{\frac{\Delta V_{bench}}{\Delta Latency}, \frac{\Delta V_{bench}}{\Delta Memory}\})$ ,

$\hat{\epsilon}_\theta \leftarrow \text{evolve}(\hat{\epsilon}_\theta, \{\hat{A}\})$

**end if**

**end while**

---



Figure A1. Comparison between the SD1.5 and our efficient spatial backbone.

## B. VAE Compression

**Separable Variational Autoencoder.** The variational autoencoder (VAE) decoder for video is more time-consuming and memory-intensive than its image counterpart, as it processes a sequence of frames as inputs. To mitigate memory consumption, we disentangle the spatial and temporal decoders to mitigate memory consumption. Specifically, given a latent feature  $\mathbf{x}_0 \in \mathbb{R}^{\tilde{n} \times 4 \times \tilde{H} \times \tilde{W}}$ , the  $\mathbf{x}_0$  is first decoded to  $\mathbf{x}_{t0} \in \mathbb{R}^{\tilde{n} \times 4 \times \tilde{H} \times \tilde{W}}$  by the temporal decoder, and then decoded back to pixel space  $\mathbf{v} \in \mathbb{R}^{\tilde{n} \times 3 \times \tilde{H} \times \tilde{W}}$  by the spatial decoder. This approach allows us to split the latent feature  $\mathbf{x}_0$  into multiple sub-features for inference, significantly reducing the peak memory. For example, a latent feature  $\mathbf{x}_0 \in \mathbb{R}^{\tilde{n} \times 4 \times \tilde{H} \times \tilde{W}}$  can be sliced to multiple sub-features with dimension  $\tilde{n}' \times 4 \times \tilde{H} \times \tilde{W}$ , where  $\tilde{n}' < \tilde{n}$ , then fed into the temporal decoder. Similarly, the temporal reconstructed latent feature, with dimension  $\tilde{n}' \times 4 \times \tilde{H} \times \tilde{W}$ , can also be fed into the spatial decoder with smaller segments such as  $1 \times 4 \times \tilde{H} \times \tilde{W}$ . This approach balances memory consumption, memory I/O, and GPU/NPU utilization, promising hardware-friendly inference.

**VAE Decoder Compression.** We conduct VAE compression only on the decoder to speed up the inference process. The encoder weights are frozen during the compression, and we only train the decoder. We replace the convolution in the original decoder with depth-wise separable convolution for better I/O and less computation. Moreover, a distill loss is adopted to maintain the reconstruction quality of the decoder. The quality comparison is shown in Tab. A1, which demonstrates our efficient decoder can achieve  $\times 54.5$  speed-up with even better performance.

VAE	Latency (s)	PSNR	SSIM	LPIPS	FloLPIPS
OpenSora	27.2	29.07	0.8066	0.1336	0.1303
Ours	0.5	29.21	0.8240	0.0949	0.0915

Table A1. Our VAE with efficient decoder.

## C. Qualitative and Quantitative Results for the Spatial Backbone

We present the qualitative results of our efficient spatial backbone, as shown in Fig. A3. These images demonstrate that our spatial backbone can achieve high-fidelity text-to-image generation quality, which promises text-to-video generation quality. We compare the CLIP-score and aesthetic score of our model with the Stable Diffusion v1.5 [45]. The evaluation is conducted on a subset of 6000 images from the MS-COCO 2014 validation set. As shown in Tab. A2, our model achieves  $\times 2.5$  compression rate while delivering better CLIP-score (0.33 vs. 0.31) and aesthetic score (6.23 vs. 5.51), exhibiting its impressive text-to-image generation quality.

Additionally, we exhibit the quality comparison of our spatial backbone with SD1.5 in Fig. A1.

Model	Params (M)	CLIP-Score $\uparrow$	Aesthetic Score $\uparrow$
SD v1.5	820	0.31	5.51
Ours	327	0.33	6.23

Table A2. Quantitative Results of Our Spatial backbone.

## D. Qualitative Comparison Results

The comparison of our model with OpenSora-v1.3[77] and CogVideoX-2B [67] is shown in Fig. A4. More comparisons are presented in [project page](#).

## E. More Qualitative Results

In this section, we present an extensive collection of qualitative results, as shown in Fig. A5, that demonstrate the capabilities of our proposed method. This includes both the examples showcased in the main paper and additional results, offering a comprehensive view of our method’s performance in various scenarios.

To facilitate a more interactive and illustrative experience, these qualitative results are provided in video format. Readers are recommended to check these results in [project page](#). This visualization provides a more nuanced understanding of the temporal and visual qualities of our method.

## F. Demo Settings

Our demo is evaluated on an iPhone 16 Pro Max, equipped with an Apple A18 Pro chipset featuring a six-core CPU, six-core GPU, and 16-core Neural Engine. Our model is converted to FP16 and executed on the Neural Engine and the CPU cores. To enhance efficiency, timestep embeddings are also pre-computed since these values are fixed for each timestep. The inference pipeline takes four denoising steps without classifier-free guidance. To enable a fast mobile

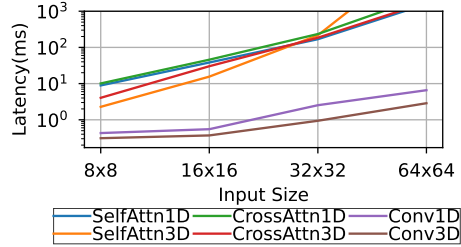


Figure A2. Latency

demo with pleasing quality, we adjust the input size for denoiser to  $15 \times 64 \times 64$ , which yields an output video clip with 51 frames  $512 \times 512$  resolution. To ensure the video quality, the model is further finetuned with video datasets with a framerate of 10 fps. Hence, the 51 frame clip is 5.1 seconds in length. Our UNet model is exported by CoreML and benchmarked using Xcode Performance tools. Furthermore, the exported model is split into two parts for loading and execution efficiency. The latency benchmark screenshots are shown in Fig. A7, thus one denoising step takes 1.02 seconds. Similarly, the text-encoder and VAE-decoder take 6 ms and 0.5 seconds, respectively. Thus, the entire inference pipeline takes less than 5 seconds on average. We exhibit the mobile demo screenshots in Fig. A6 and [project page](#).

## G. Effect of Adversarial Fine-tuning

Tab. 5 also shows the effect of adversarial fine-tuning. Tuning without adversarial loss can not yield promising results compared to the baseline for step distillation.

## H. Latency Analysis

The latency of different temporal blocks is shown in Fig. A2.



*"Golden Retriever and French Bulldog go through a dark corridor of abandoned alien spacecraft. Sci-fi horror movie style, ..."*



*"A busy medieval marketplace, wooden stalls filled with goods, people in period attire bustling about. A blacksmith's shop is seen in the distance ..."*



*"A space girl posing in the street, wearing a spacesuit and a helmet without visor, camera rapidly fast dolly with focus on her face, bokeh and flares, chromatic aberration."*



*"A woman is shopping for fresh produce at a farmer's market"*



*"A cat, beautiful gorgeous lush summer garden, a cute red cat hunts and jumps in the flowers, soft focus soft warm color correction."*



*"Mr. Hamster, a red-haired, chubby rodent, dressed as a great artist, holding a brush and writing his masterpiece on an easel, is on the surface of the moon."*



*"A realistic purple-haired girl with freckles a bit and purple lips, recording blog and looking at the camera and smiling, beautiful green eyes in a modern studio with a professional cameras and filmmaking equipment behind."*



*"a shot of a city completely overgrown by bright orange plants. Giant orange mushrooms are seen among the cityscapes. Orange ivy covers the buildings, orange moss covers the streets ..."*



*"Camera aerial horizon shot: pyramids in the desert, rockets launch from spaceport among structures."*



*"A lady with brown hair puts on a short yellow dress. Plush red carpet and yellow wallpaper with swirling pattern. Interior shot of a grand, hotel room."*



*"Tilt-shift wide shot, panning upwards moving camera. Nighttime scene with Petronas Towers lit up, surrounded by bamboo and salvia. Symmetrical, Malaysian-inspired architecture with a massive, tall gate ..."*



*"A girl is standing and looking to the camera in a fashion coat, night city and streets."*



*"A large UFO hovers above a deserted road winding through a barren, mountainous landscape. The black and white tones evoke a classic, documentary atmosphere."*



*"A panda with a red backpack is walking through the snow, captured in an inspirational travel movie style with dark teal and light red color correction."*



*"In the center of the frame. A small orange bird is perched gracefully on the branch, presented in a vibrant, photorealistic style that highlights the bird's striking color against the fresh green foliage."*



*"A bustling cityscape at sunset with skyscrapers reflecting golden light, people walking, and traffic moving swiftly."*

**Figure A3. Qualitative results of the spatial backbone.**

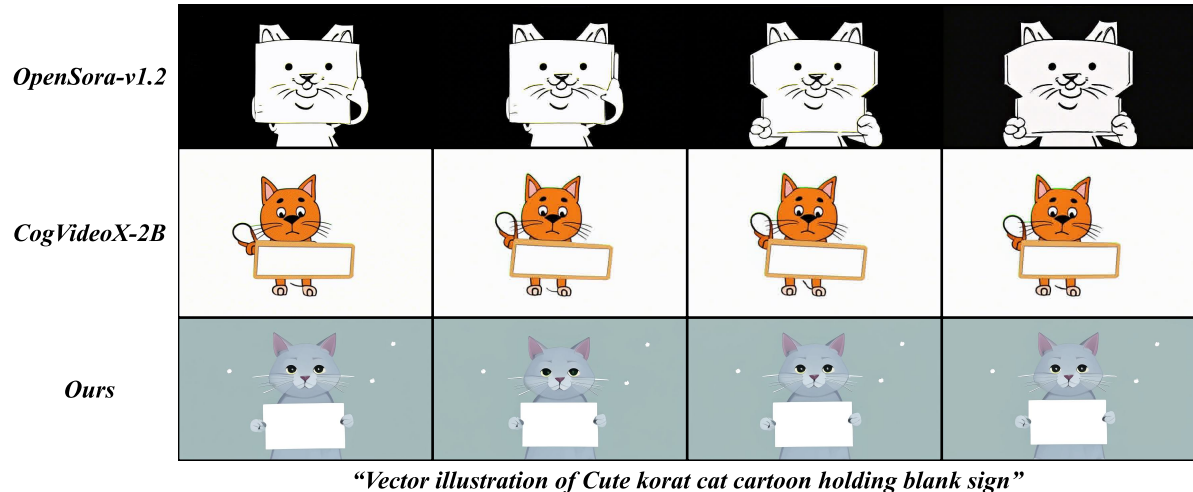


Figure A4. Comparison with OpenSora-v1.2 [77] and CogVideoX-2B [67].

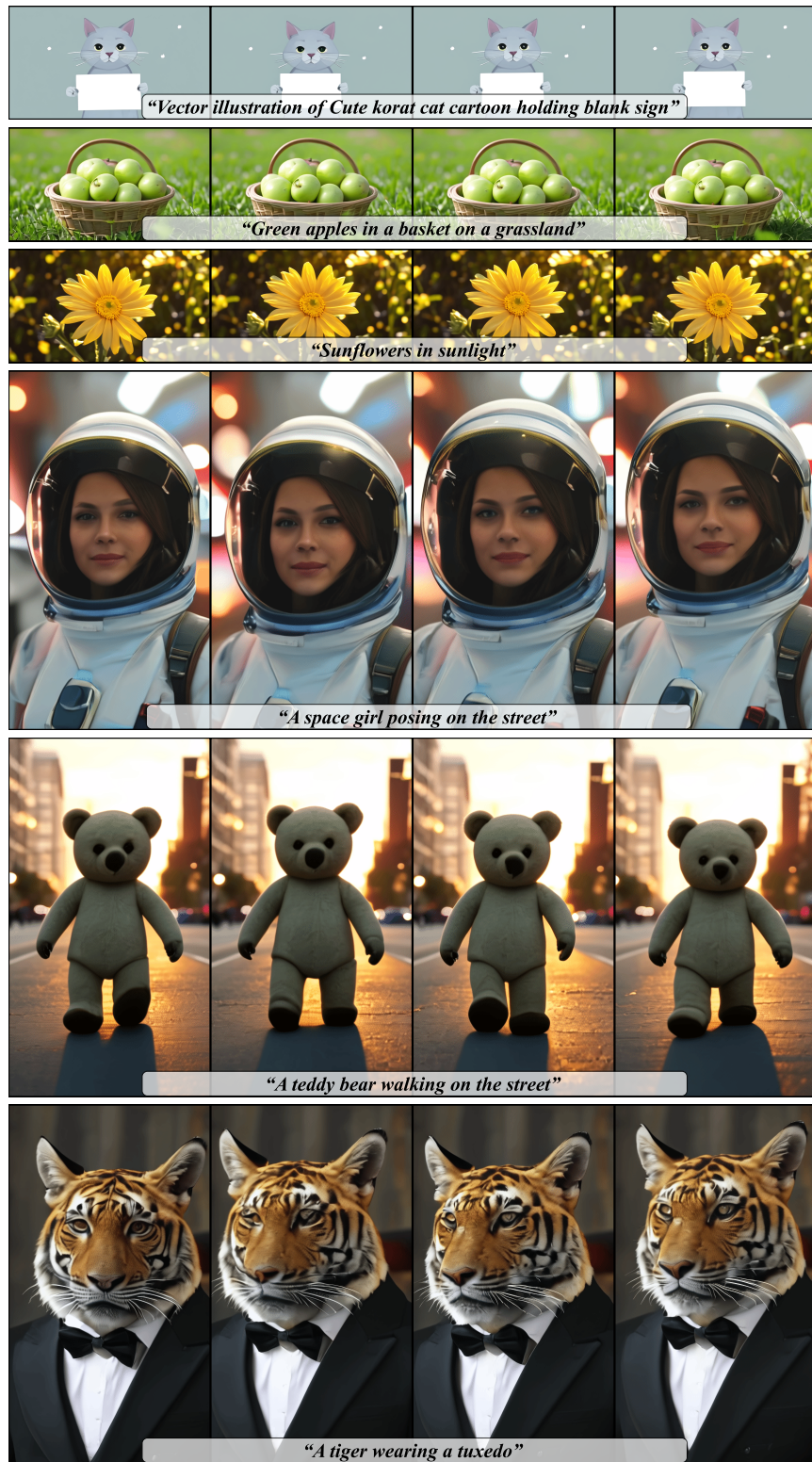


Figure A5. More qualitative results.

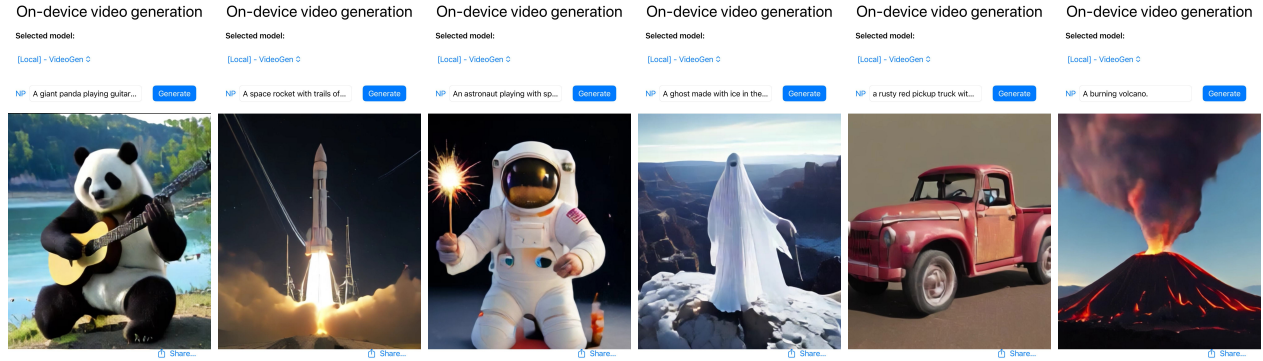


Figure A6. Screenshots of Mobile Demo.

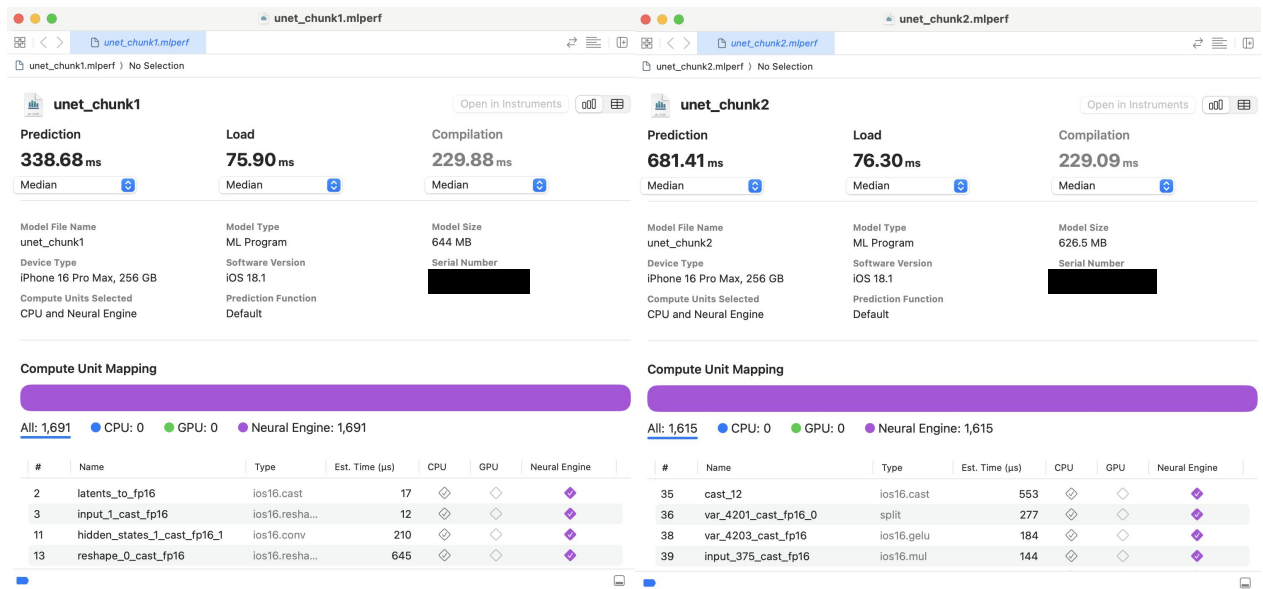


Figure A7. UNet Latency Benchmark on iPhone 16 Pro Max.